

REPORT DOCUMENTATION PAGE			Form Approved OMB NO. 0704-0188	
<p>The public reporting burden for this collection of information is estimated to average 1 hour per response, including the time for reviewing instructions, searching existing data sources, gathering and maintaining the data needed, and completing and reviewing the collection of information. Send comments regarding this burden estimate or any other aspect of this collection of information, including suggestions for reducing this burden, to Washington Headquarters Services, Directorate for Information Operations and Reports, 1215 Jefferson Davis Highway, Suite 1204, Arlington VA, 22202-4302. Respondents should be aware that notwithstanding any other provision of law, no person shall be subject to any penalty for failing to comply with a collection of information if it does not display a currently valid OMB control number.</p> <p>PLEASE DO NOT RETURN YOUR FORM TO THE ABOVE ADDRESS.</p>				
1. REPORT DATE (DD-MM-YYYY)		2. REPORT TYPE		3. DATES COVERED (From - To)
		New Reprint		-
4. TITLE AND SUBTITLE			5a. CONTRACT NUMBER	
Development of a Robust and Cost-Effective Friction Stir Welding Process for Use in Advanced Military Vehicles			W911NF-11-1-0207	
			5b. GRANT NUMBER	
			5c. PROGRAM ELEMENT NUMBER	622105
6. AUTHORS			5d. PROJECT NUMBER	
M. Grujicic, G. Arakere, B. Pandurangan, A. Hariharan, C.-F. Yen, B. A. Cheeseman			5e. TASK NUMBER	
			5f. WORK UNIT NUMBER	
7. PERFORMING ORGANIZATION NAMES AND ADDRESSES			8. PERFORMING ORGANIZATION REPORT NUMBER	
Clemson University Office of Sponsored Programs 300 Brackett Hall Clemson, SC 29634 -5702				
9. SPONSORING/MONITORING AGENCY NAME(S) AND ADDRESS(ES)			10. SPONSOR/MONITOR'S ACRONYM(S) ARO	
U.S. Army Research Office P.O. Box 12211 Research Triangle Park, NC 27709-2211			11. SPONSOR/MONITOR'S REPORT NUMBER(S) 57228-EG.4	
12. DISTRIBUTION AVAILABILITY STATEMENT Approved for public release; distribution is unlimited.				
13. SUPPLEMENTARY NOTES The views, opinions and/or findings contained in this report are those of the author(s) and should not be construed as an official Department of the Army position, policy or decision, unless so designated by other documentation.				
14. ABSTRACT To respond to the advent of more lethal threats, recently designed aluminum-armor-based military-vehicle systems have resorted to an increasing use of higher strength aluminum alloys (with superior ballistic resistance against armor piercing (AP) threats and with high vehicle-light weighing potential). Unfortunately, these alloys are not very amenable to conventional fusion-based welding technologies and in-order to obtain high-quality welds, solid-state joining technologies such as Friction stir welding (FSW) have to be				
15. SUBJECT TERMS aluminum, automotive, joining, welding				
16. SECURITY CLASSIFICATION OF:			17. LIMITATION OF ABSTRACT	15. NUMBER OF PAGES
a. REPORT	b. ABSTRACT	c. THIS PAGE	UU	19a. NAME OF RESPONSIBLE PERSON
UU	UU	UU		Mica Grujicic
				19b. TELEPHONE NUMBER
				864-656-5639

## **Report Title**

Development of a Robust and Cost-Effective Friction Stir Welding Process for Use in Advanced Military Vehicles

### **ABSTRACT**

To respond to the advent of more lethal threats, recently designed aluminum-armor-based military-vehicle systems have resorted to an increasing use of higher strength aluminum alloys (with superior ballistic resistance against armor piercing (AP) threats and with high vehicle-light weighing potential). Unfortunately, these alloys are not very amenable to conventional fusion-based welding technologies and in-order to obtain high-quality welds, solid-state joining technologies such as Friction stir welding (FSW) have to be employed. However, since FSW is a relatively new and fairly complex joining technology, its introduction into advanced military vehicle structures is not straight forward and entails a comprehensive multi-step approach. One such (three-step) approach is developed in the present work. Within the first step, experimental and computational techniques are utilized to determine the optimal tool design and the optimal FSW process parameters which result in maximal productivity of the joining process and the highest quality of the weld. Within the second step, techniques are developed for the identification and qualification of the optimal weld joint designs in different sections of a prototypical military vehicle structure. In the third step, problems associated with the fabrication of a sub-scale military vehicle test structure and the blast survivability of the structure are assessed. The results obtained and the lessons learned are used to judge the potential of the current approach in shortening the development time and in enhancing reliability and blast survivability of military vehicle structures.



---

**REPORT DOCUMENTATION PAGE (SF298)**  
**(Continuation Sheet)**

---

Continuation for Block 13

ARO Report Number 57228.4-EG  
Development of a Robust and Cost-Effective Fri ...

Block 13: Supplementary Note

© 2011 . Published in Journal of Materials Engineering and Performance, Vol. Ed. 0 20, (1) (2011), (, (1). DoD Components reserve a royalty-free, nonexclusive and irrevocable right to reproduce, publish, or otherwise use the work for Federal purposes, and to authorize others to do so (DODGARS §32.36). The views, opinions and/or findings contained in this report are those of the author(s) and should not be construed as an official Department of the Army position, policy or decision, unless so designated by other documentation.

Approved for public release; distribution is unlimited.

# Development of a Robust and Cost-Effective Friction Stir Welding Process for Use in Advanced Military Vehicles

M. Grujicic, G. Arakere, B. Pandurangan, A. Hariharan, C.-F. Yen, and B.A. Cheeseman

(Submitted February 5, 2010)

To respond to the advent of more lethal threats, recently designed aluminum-armor-based military-vehicle systems have resorted to an increasing use of higher strength aluminum alloys (with superior ballistic resistance against armor piercing (AP) threats and with high vehicle-light weighing potential). Unfortunately, these alloys are not very amenable to conventional fusion-based welding technologies and in-order to obtain high-quality welds, solid-state joining technologies such as Friction stir welding (FSW) have to be employed. However, since FSW is a relatively new and fairly complex joining technology, its introduction into advanced military vehicle structures is not straight forward and entails a comprehensive multi-step approach. One such (three-step) approach is developed in the present work. Within the first step, experimental and computational techniques are utilized to determine the optimal tool design and the optimal FSW process parameters which result in maximal productivity of the joining process and the highest quality of the weld. Within the second step, techniques are developed for the identification and qualification of the optimal weld joint designs in different sections of a prototypical military vehicle structure. In the third step, problems associated with the fabrication of a sub-scale military vehicle test structure and the blast survivability of the structure are assessed. The results obtained and the lessons learned are used to judge the potential of the current approach in shortening the development time and in enhancing reliability and blast survivability of military vehicle structures.

**Keywords** aluminum, automotive, joining, welding

## 1. Introduction

Friction stir welding (FSW) is a solid-state metal-joining process that was invented in 1991 at The Welding Institute in the United Kingdom (Ref 1). FSW can be used to produce butt, corner, lap, T, spot, fillet, and hem joints, as well as to weld hollow objects, such as tanks and tubes/pipes, stock with different thicknesses, tapered sections and parts with three-dimensional contours. This welding process is particularly suited for butt and lap joining of aluminum alloys which are otherwise quite difficult to join using conventional arc/fusion welding processes. FSW has established itself as a preferred joining technique for aluminum components and its applications for joining other *difficult-to-weld* metals are gradually expanding. Currently, this joining process is being widely used in many industrial sectors such as shipbuilding and marine, aerospace, railway, land transportation, etc.

The basic concept behind FSW is described using the example of butt welding, Fig. 1. As shown in Fig. 1, a non-consumable rotating tool moves along the contacting surfaces of

two rigidly butt-clamped plates. As seen in this figure, the tool consists of a cylindrical pin which is threaded, at one end, and equipped with a shoulder, at the other. Also, during joining, the work-piece (i.e., the two clamped plates) is generally placed on a rigid backing support. At the same time, the shoulder is forced to make a firm contact with the top surface of the work-piece. As the tool rotates and moves along the butting surfaces, heat is being generated at the shoulder/work-piece and, to a lesser extent, at the pin/work-piece contact surfaces, as a result of the frictional-energy dissipation. This, in turn, causes an increase in temperature and gives rise to softening of the material adjacent to these contacting surfaces. As the tool advances along the butting surfaces, thermally softened material in front of the tool is (heavily) deformed, extruded around the tool to the region behind the tool and compacted/forged to form a joint/weld.

Relative to the traditional fusion-welding technologies, FSW offers a number of advantages such as:

- good mechanical properties in the *as-welded* condition and substantial improvements in the consistency of weld quality (even in those alloys that are considered non-weldable by conventional techniques);
- improved safety due to the absence of toxic fumes or the spatter of molten material;
- no consumables such as the filler metal or gas shield are required;
- ease of process automation;
- ability to operate in all positions (horizontal, vertical, overhead, orbital, etc.), as there is no weld pool;
- minimal thickness under/over-matching which reduces the need for expensive post-weld machining;
- low environmental impact;

M. Grujicic, G. Arakere, B. Pandurangan, and A. Hariharan, Department of Mechanical Engineering, Clemson University, Clemson, SC 29634; and C.-F. Yen and B.A. Cheeseman, Army Research Laboratory, Survivability Materials Branch, Aberdeen, Proving Ground, MD 21005-5069. Contact e-mails: mica.grujicic@ces.clemson.edu and mica@ces.clemson.edu.



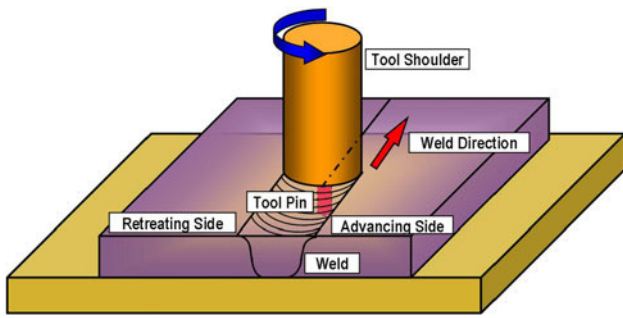


Fig. 1 A schematic of the friction stir welding (FSW) process

- (h) aluminum-alloy welds in a 0.02-3.0 in range can be produced and, typically, in a single pass;
- (i) dissimilar aluminum-alloy grades (e.g., AA6061 to AA5083), wrought and cast aluminum alloys, as well as aluminum matrix composites can be readily FSWed;
- (j) due to lower attendant temperatures, the residual stresses and distortions are substantially reduced in comparison to those encountered in traditional arc welding processes;
- (k) the innermost zone of the FSW joint typically consists of a fine equiaxed grain structure which may possess superior impact resistance properties;
- (l) a complete absence of filler-induced defects (since, FSW is a filler-less process) and hydrogen-embrittlement cracking (since no hydrocarbon fuel is used);
- (m) the joining process can be carried out by using modified traditional machine tool technologies;
- (n) replacement of fastened joints with FSW joints can lead to significant weight reduction and cost savings;
- (o) since FSW is a solid-state process, the joint is free of solidification-induced defects and, consequently, certain 2xxx and 7xxx aluminum alloys which are difficult to join using conventional fusion welding processes can be readily FSWed.

Unfortunately, the FSW technology is burdened by several disadvantages such as:

- (a) an exit hole is left after the tool is withdrawn from the work-piece;
- (b) relatively large tool press-down and plates-clamping forces are required;
- (c) lower flexibility of the process with respect to variable-thickness and non-linear welds;
- (d) often associated with lower welding rates than conventional fusion-welding techniques, although this shortcoming is somewhat lessened since fewer welding passes are required; and
- (e) FSW equipment cost is typically significantly higher than the equipment cost encountered in most traditional fusion welding processes. This disadvantage is somewhat mitigated by the associated lower labor cost and by a lower need for skilled labor.

Recent efforts of the U.S. Army have been aimed at becoming more mobile, deployable, and sustainable while maintaining or surpassing the current levels of lethality and survivability. Current battlefield vehicles have reached in excess of 70 tons due to ever increasing lethality of ballistic

threats which hinders their ability to be readily transported and sustained. Therefore, a number of research and development programs are under way to engineer light-weight, highly mobile, transportable, and lethal battlefield vehicles with a target weight under 20 tons. To attain these goals, significant advances are needed in the areas of light-weight structural- and armor-materials development (including aluminum-based structural/armor-grade materials).

Historically, aluminum alloy AA5083-H131 has been used in military-vehicle systems such as the M1113 and the M109, in accordance with the MIL-DTL-46027J specification (Ref 2). The main reasons for the selection of this alloy are its lighter weight, ease of joining by various welding techniques, a relatively high level of performance against fragmentation-based threats, and superior corrosion resistance.

To respond to the advent of more lethal threats, recently designed aluminum-armor-based military-vehicle systems, such as the M2 Bradley Fighting Vehicle, have relied on the use of higher strength aluminum alloys, such as AA2139 (Ref 3), AA7039 (Ref 4), AA2219 (Ref 5), and AA2519 (Ref 6). These alloys provide increased ballistic protection against armor piercing (AP) threats due to their higher dynamic strength. In addition, higher quasi-static tensile strength levels offered by these alloys are very desirable for vehicle-hull designs as they enable significant reductions in the vehicle weight. However, these alloys also show some significant shortcomings primarily due to their lower fusion-based weldability and inferior corrosion resistance in comparison to that observed in AA5083-H131. Fortunately, there are efficient remedies for these shortcomings: The low corrosion-resistance shortcomings can be, in general, overcome through the use of various coating and cladding technologies (not the subject of the present work), while the low weldability shortcomings can be addressed using FSW (the main subject of the present work). However, since FSW is a relatively new and fairly complex joining technology, its introduction into advanced military vehicle structures is not straight forward and entails a comprehensive multi-prong approach. Development of one such approach is the subject of the present work.

Within the present approach, the three main stages for the introduction of FSW process into advanced military vehicle structures are identified as:

- (a) Determination of the optimal tool design and the optimal FSW process parameters which result in maximal productivity of the joining process (as measured by the tool travel speed) and the highest quality of the weld (as quantified by the weld mechanical properties and their reproducibility), for a given choice of the high-strength aluminum-alloy grades being welded. As will be shown later, at this stage the traditional experimentally based process-development efforts are complimented by an extensive program of weld-material property characterization/testing and thermal/mechanical computational analyses which can help establish correlations between the FSW process parameters and the weld microstructure/mechanical properties;
- (b) Identification of the optimal weld joint design for different sections of the military vehicle structures and employment of experimental test procedures (e.g., ballistic shock test, discussed later) to qualify the welded joints; and
- (c) Fabrication of a sub-scale military vehicle test structure and the employment of experimental techniques to access their blast survivability.

185 The organization of the paper is as follows: A detailed  
 186 description of the FSW process parameters (including weld tool  
 187 geometry), weld material microstructure spatial distribution and  
 188 temporal evolution as well as correlations between the FSW  
 189 process parameters and the weld-material microstructure/  
 190 properties are all discussed in Section 2. Details pertaining to  
 191 the design and testing of FSW joints for use in military vehicle  
 192 structures are presented in Section 3. A brief discussion  
 193 regarding the fabrication and blast-survivability testing of the  
 194 sub-scale military vehicle test structure is provided in Sec-  
 195 tion 4. It should be noted that due to the sensitive nature of the  
 196 subject matter and for the potential misuse of the findings  
 197 obtained in the present work, some critical quantitative results  
 198 had to be left out. The main conclusions resulting from the  
 199 present study are summarized in Section 5.

## 200 2. FSW Process and Weld Joint Material Analysis

### 201 2.1 FSW Process

202 **2.1.1 Mass/Heat Transport and Thermo-mechanical**  
 203 **Aspects.** FSW normally involves complex interactions and  
 204 competition between various thermo-mechanical processes  
 205 such as frictional-energy dissipation, plastic deformation, and  
 206 the associated heat dissipation, material transport/flow, dynamic  
 207 recrystallization, local cooling, etc. (Ref 7-14). A unique  
 208 feature of the FSW process is that heat transfer does not only  
 209 take place via thermal conduction but also via transport of the  
 210 work-piece material adjacent to the tool from the region in front  
 211 to the region behind the advancing tool. In general both the heat  
 212 and the mass transfer depend on the work-piece material  
 213 properties, tool geometry, and the FSW process parameters. As  
 214 will be discussed later in greater details, mass transport is  
 215 accompanied by extensive plastic deformation and dynamic  
 216 recrystallization of the transported material. The attendant  
 217 strain rates as high as  $10 \text{ s}^{-1}$  have been assessed/measured  
 218 (Ref 15, 16).

219 **2.1.2 Process Parameters.** The main FSW process  
 220 parameters which affect both the weld quality and the process  
 221 efficiency are: (a) rotational and transverse velocities of the  
 222 tool; (b) tool-plunge depth; (c) tool tilt-angle; and (d) tool-  
 223 design/material. Since, in-general, higher temperatures are  
 224 encountered in the case of higher rotational and lower  
 225 transverse tool velocities, it is critical that a delicate balance  
 226 between these two velocities is attained. In other words, when  
 227 the temperatures are not high enough and the material has not  
 228 been sufficiently softened, the weld zone may develop various  
 229 flaws/defects arising from low ductility of the material.  
 230 Conversely, when the temperatures are too high undesirable  
 231 changes in the material microstructure/properties may take  
 232 place and possibly incipient-melting flaws may be created  
 233 during joining. To ensure that the necessary level of shoulder/  
 234 work-piece contact pressure is attained and that the tool fully  
 235 penetrates the weld, the tool-plunge depth (defined as the depth  
 236 of the lowest point of the shoulder below the surface of the  
 237 welded plate) has to be set correctly. Typically, insufficient tool-  
 238 plunge depths result in low-quality welds (due to inadequate  
 239 forging of the material at the rear of the tool), while excessive  
 240 tool-plunge depths lead to under-matching of the weld thick-  
 241 ness compared to the base-materials thickness. Tool rearward  
 242 tilting by 2-4 degrees has been often found to be beneficial  
 243 since it enhances the effect of the forging process.

244 Tool design is one of the most important factors that  
 245 influences the FSW joint profile as well as the weld material  
 246 microstructure and properties. Initially, one-piece steel tools  
 247 were used with both the pin and the shoulder having a (smooth-  
 248 surface) right circular cylindrical geometry. Consequently, only  
 249 limited material flow and mixing were produced. The two-piece  
 250 FSW tools used today typically contain (flat-ended) threaded,  
 251 fluted, and/or frustum (with flats) pin designs which promote  
 252 material transport around the tool as well as in the work-piece  
 253 through-the-thickness direction. This, in turn, enables higher  
 254 weld speeds and higher quality void free weld joints. In  
 255 addition, current FSW tools contain scrolled shoulders which  
 256 eliminates the need for the aforementioned tool tilting (facilitate  
 257 welding around corners and production of non-linear welds),  
 258 weld surface undercutting and the flash that extrudes under the  
 259 tool shoulder. Novel FSW tools often contain non-circular (e.g.,  
 260 oval, paddle, etc.) cross sections to increase the volume of  
 261 stirred material and improve weld properties. Tool design is  
 262 probably the most guarded secret in FSW community, as  
 263 companies/researchers are generally reluctant to disclose tool-  
 264 ing information.

265 **2.1.3 Weld Advancing and Retreating Sides.** When  
 266 analyzing the FSW process, one often makes a distinction  
 267 between the so-called *advancing* side of the weld (the side on  
 268 which the peripheral velocity of the rotating tool coincides with  
 269 the transverse velocity of the tool) and the *retreating* side (the  
 270 side on which the two velocities are aligned in the opposite  
 271 directions). It is generally recognized that the differences in the  
 272 two weld sides give rise to asymmetry in heat transfer, material  
 273 flow, and weld microstructure-properties (Ref 17).

### 274 2.2 Weld Material Microstructure/Property Distribution 275 and Evolution

276 **2.2.1 Weld Zones and Associated Microstructure Char-  
 277 acteristics.** Metallographic examinations of the FSW joints  
 278 typically reveal the existence of the following four zones,  
 279 Fig. 2:

- 280 (a) an un-effected zone which is far enough from the weld  
 281 so that material microstructure/properties are not altered  
 282 by the joining process;  
 283 (b) the heat-affected zone (HAZ) in which material micro-  
 284 structure/properties are effected only by the thermal ef-  
 285 fects associated with FSW. While this zone is normally  
 286 found in the case of fusion-welds, the nature of the  
 287 microstructural changes may be different in the FSW  
 288 case due to generally lower temperatures and a more  
 289 diffuse heat source;  
 290 (c) the thermo-mechanically affected zone (TMAZ) which  
 291 is located closer than the HAZ zone to the butting

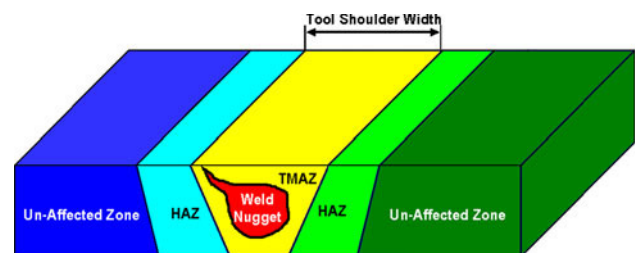


Fig. 2 A schematic of the four microstructural zones associated with the typical FSW joint

surfaces. Consequently both the thermal and the mechanical aspects of the FSW affect the material microstructure/properties in this zone. Typically, the original grains are retained in this zone although they may have undergone severe plastic deformation; and

(d) the weld *nugget* is the innermost zone of an FSW joint. As a result of the way the material is transported from the regions ahead of the tool to the wake regions behind the tool, this zone typically contains the so called “*onion-ring*” features. The material in this region has been subjected to most severe conditions of plastic deformation and high temperature exposure and consequently contains a very-fine dynamically recrystallized equiaxed grain microstructure.

**2.2.2 Weld Microstructure Evolution During FSW Process.** As clearly demonstrated in our prior work (Ref 18), while weld-microstructure evolution will vary with the choice of base materials and FSW process parameters, these changes show some clear differences between non-heat treatable (non age-hardenable) and heat treatable aluminum-alloy grades. Specifically, in the case of non-age-hardenable alloys (e.g., AA5083), the dominant microstructure evolution processes taking place during FSW are extensive plastic deformation and dynamic recrystallization of highly deformed material subjected to elevated temperatures approaching the solidus temperature of the alloy. On the other hand, in the case of age-hardenable alloys (e.g., AA2139), in addition to plastic deformation and dynamic recrystallization, precipitate coarsening, over-aging, dissolution, and re-precipitation typically take place.

**2.2.3 Weld Microstructure/Property Relations.** Taking into account the basic physical metallurgy aspects of the alloys being welded and considering the aforementioned spatial distribution and temporal evolution of the weld-material microstructure, it is to be expected that local material properties (in particular mechanical properties) may vary over the weld joint.

In the case of non-heat treatable aluminum alloys material strength (and ductility) is controlled by the following strengthening mechanisms:

- (a) *Solid Solution Strengthening:* This hardening mechanism is present in all four weld-zones and its contribution to the material hardness is expected to be fairly uniform across the entire weld region;
- (b) *Strain Hardening:* When a non-heat treatable alloy is cold worked, strain hardening mechanism provides a contribution to the material hardness in the base-metal zone which is larger than the contributions of the other two mechanisms. In the HAZ, some annealing will take place. However, since this annealing is primarily due to recovery or polygonization, the contribution of strain hardening to the material hardness in this region will remain quite comparable to that in the base metal region. The contribution of strain hardening to the overall material hardness in the TMAZ is expected to increase since the material in this region typically experiences significant levels of plastic deformation. In the weld nugget region, material microstructure and properties are dominated by dynamic recrystallization and, hence, the contribution of strain hardening to the overall material hardness in this region is minimal; and

- (c) *Grain Size Refinement:* Since, to a first-order approximation, the average grain size does not change between the base-metal zone, the HAZ and the TMAZ, the contribution of this strengthening mechanism to the overall material strength is expected to be comparable in these three weld-zones. On the other hand, dynamic recrystallization yields a very fine grain structure within the nugget zone so that the overall contribution of the grain-refinement mechanism to the material hardness is expected to be largest in this weld zone.

In the case of heat treatable aluminum alloys material strength (and ductility) is controlled by the following strengthening mechanisms: (a) precipitation hardening; (b) strain hardening; and (c) grain-size refinement. Relative importance of the strain hardening and the grain-size refinement mechanisms within the four weld-zones was discussed earlier in the context of non-heat treatable alloys. The main points made at that time are equally valid in the case of heat-treatable alloys. As far as the role of the precipitation hardening mechanism in heat-treatable alloys is concerned, the following main observations can be made. Typically in heat-treatable alloys, precipitation hardening provides a contribution to the material hardness in the base-metal zone which is larger than the contributions of the other two mechanisms. In general, material exposure to high-temperatures within the remaining three main weld-zones causes over-aging and the associated loss in material strength. This loss increases in its extent as one approaches the original weld-line, i.e., as one moves through the HAZ, then through the TMAZ and ultimately through the weld nugget.

## 2.3 Correlation Between FSW-Process Parameters and Weld Joint Material Performance

**2.3.1 Experimental Approach.** Over the last two decades, considerable experimental research efforts have been invested toward providing a better understanding of the FSW joining mechanism and the accompanying evolution of the welded-materials microstructure/properties (e.g. Ref 19-22) as well as to rationalizing the effect of various FSW process parameters on the weld quality/integrity (e.g. Ref 10, 23-25). It should be recognized, however, that the aforementioned experimental efforts were able to only correlate the *post-mortem* welded-materials microstructure/properties with the FSW process parameters and provided relatively little real-time insight into the physics of heat/mass transfer and microstructure-evolution processes. As shown in our previous work (Ref 26), this insight can be gained by carrying out a detailed physically based computational analysis of the FSW process. Nevertheless, experimental techniques involving weld-material microstructure and property characterizations for FSW joints obtained under various combinations of process parameters and the tool geometry remain invaluable for calibration and validation of the aforementioned computational-based analyses. The weld material microstructure characterization techniques typically include optical, scanning-electron and transmission-electron microscopies, and x-ray diffraction analysis. Among the weld-material mechanical property characterization techniques the most widely used are transverse tensile tests, all-weld longitudinal tensile test and a transverse bend test (Ref 27).

**2.3.2 Computational Approach.** A detailed review of the prior research efforts dealing with computational investigations of the FSW process reported in the public domain



413 literature was conducted in our previous work (Ref 26). Hence,  
 414 no overview of the prior computational FSW research efforts  
 415 will be presented here. Instead, a brief overview will be  
 416 provided of our recent fully coupled thermo-mechanical finite-  
 417 element analysis of the FSW process which combines the mass,  
 418 momentum, and heat-transfer conservation equations with the  
 419 basic physical metallurgy (microstructure evolution) of the  
 420 aluminum alloy grades being FSWed (Ref 26). Within this  
 421 analysis, various microstructure-evolution processes taking  
 422 place during FSW (e.g., extensive plastic-deformation induced  
 423 grain-shape distortion and dislocation-density increase,  
 424 dynamic recrystallization, and precipitates coarsening, over-  
 425 aging, dissolution, and re-precipitation) are considered to  
 426 predict the material microstructure/properties in the various  
 427 FSW zones of the alloys being welded. For each of the  
 428 aforementioned microstructure evolution processes, the appro-  
 429 priate material state variables are introduced and their evolution  
 430 equations constructed and parameterized (using available open  
 431 literature sources pertaining to the kinetics of the microstructure  
 432 evolution processes). Next, the thermo-mechanical constitutive  
 433 model for the alloys being FSWed is modified to include the  
 434 effect of the local material microstructure. This procedure  
 435 enabled examination of the two-way interactions between the  
 436 FSW process and the weld-material microstructure evolution.  
 437 In other words, both the effect of the current material  
 438 microstructure on its thermo-mechanical response during the  
 439 FSW process and the effects of thermo-mechanical history of a  
 440 material point during the FSW process on the associated  
 441 microstructure could be analyzed.

442 In the remainder of this section a few typical FSW process  
 443 simulation results obtained using our FSW model (Ref 26) are  
 444 presented and briefly discussed.

445 *Equivalent Plastic Strain Field.* An example of the typical  
 446 results pertaining to spatial distribution and temporal evolution  
 447 of the equivalent plastic strain in the work-piece during FSW is  
 448 displayed in Fig. 3(a-d). Simple examination of the results like  
 449 the ones displayed in these figures but generated under different  
 450 FSW process conditions reveals that: (a) depending on the FSW  
 451 process conditions such as tool contact pressure, tool rotational

452 and translational speeds, equivalent plastic strains in a range  
 453 between 20 and 50 are observed; (b) the highest equivalent  
 454 plastic strains are always found in the work-piece material  
 455 right below the tool shoulder and equivalent plastic strains  
 456 progressively decreased from this region as a function of the  
 457 distance in the radial and through-the-thickness directions;  
 458 (c) there is a highly pronounced asymmetry in the distribu-  
 459 tion of the equivalent plastic strain relative to the initial  
 460 location of the butting surfaces. This asymmetry is related to  
 461 the aforementioned differences in the material transport (at  
 462 the advancing and the retreating sides of the weld) from the  
 463 region ahead of the tool to the region behind the tool; and  
 464 (d) as the tool translational speed is decreased and the tool/  
 465 work-piece contact pressure is increased, higher equivalent  
 466 plastic strains are observed and equivalent plastic strain  
 467 differences between the top and bottom surfaces of the work  
 468 piece are reduced. This finding suggests that under these  
 469 FSW process conditions the extent of material stirring/mixing  
 470 (which plays a critical role in weld quality/joint-strength) is  
 471 increased.

472 *Nodal Velocity Field.* The distribution of nodal velocities at the  
 473 outer surfaces of the work-piece at two different times (0.0 and  
 474 0.5 s) is displayed in Fig. 4(a-b). For clarity, the tool is not  
 475 shown. These figures clearly show that the initially assigned  
 476 unidirectional velocity field (to the work-piece material within  
 477 the Arbitrary-Lagrangian-Eulerian (ALE) finite-element formu-  
 478 lation used in Ref 26) in the direction of welding, quickly  
 479 transforms into the velocity field in which there is a well-  
 480 defined stir region right below the shoulder (within which the  
 481 material circles around the pin) and the remainder of the field  
 482 (within which the material tends to flow around the stir region).  
 483 A comparison of the results displayed in Fig. 4(a-b) clearly  
 484 shows how the region underneath the tool shoulder which is  
 485 initially unfilled becomes filled as FSW proceeds (please note  
 486 an increase in the work-piece hole upper-rim altitude). Once the  
 487 space under the shoulder is fully filled it remains filled as the  
 488 FSW process continues. The material in this region is  
 489 constantly being refreshed as the tool advances in the welding  
 490 direction.

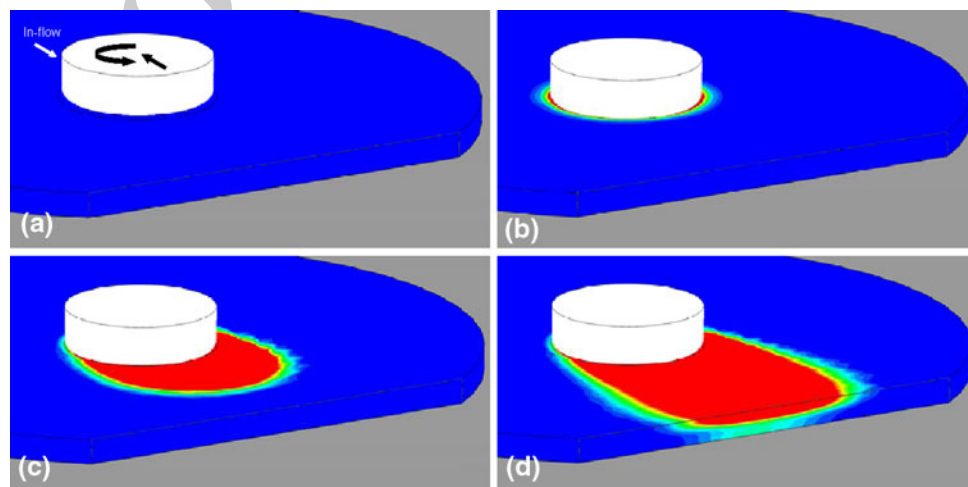
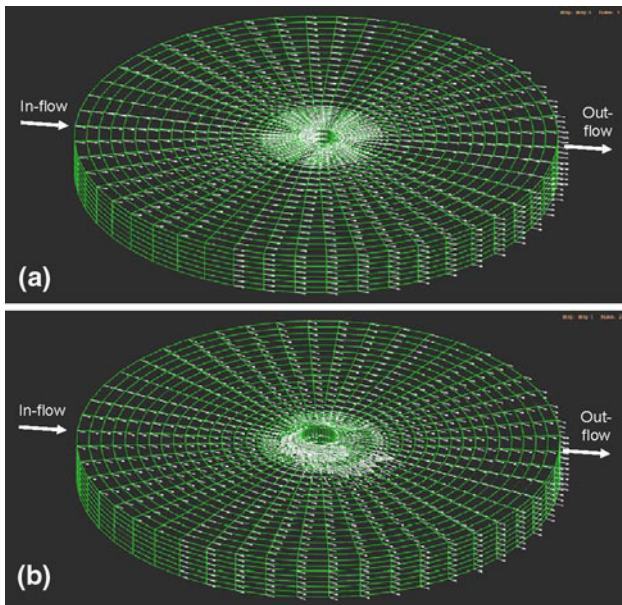
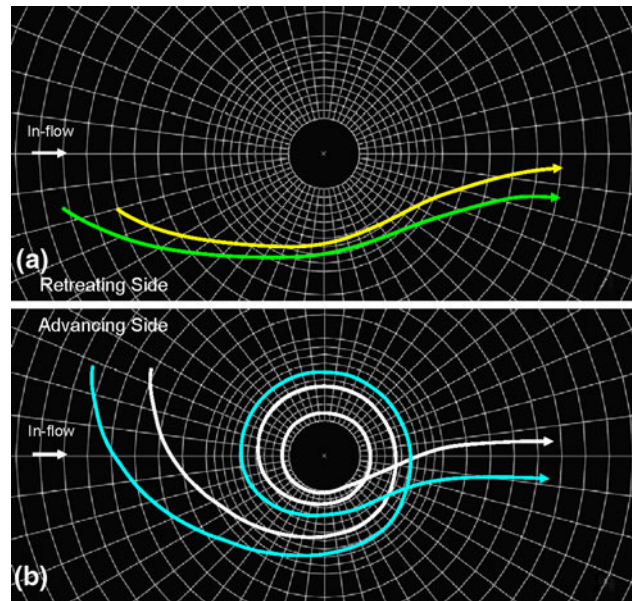


Fig. 3 Typical results pertaining to spatial distribution and temporal evolution of the equivalent plastic strain during FSW: (a) zero-time step; (b) at the end of tool-insertion; (c) 7 s afterwards; and (d) 14 s afterwards. Equivalent-plastic strain range: 0.0 (blue) to 50.0 (red)



**Fig. 4** A typical nodal-velocity field associated with friction stir welding: (a) the initial state; (b) the fully developed state



**Fig. 5** (a) Retreating-side and (b) advancing-side tracer-particle typical trajectories

491 *Material/Tracer Particle Trajectories.* The results displayed in  
 492 Fig. 4(a-b) show the spatial distribution and temporal evolution  
 493 of the nodal velocities. It should be noted that due to the ALE  
 494 character of the finite-element analysis used in Ref 26, the  
 495 motion of the finite-element mesh is not completely tied to  
 496 the motion of the material. Thus, the results displayed in  
 497 Fig. 4(a-b) show the velocities of the material particles which  
 498 at that moment pass through the nodal points in question.  
 499 However, at different times different material particles are  
 500 associated with the same nodes. To observe material extrusion  
 501 around the tool pin and its forging at the tool wake, it is more  
 502 appropriate to construct and analyze material-particle trajec-  
 503 tories. This was made possible within ABAQUS/Explicit finite  
 504 element code employed in Ref 26 through the use of so-called  
 505 “tracer particles” which are attached to the material points  
 506 (and not to the mesh nodal points).

507 An example of the prototypical results pertaining to the  
 508 trajectory of retreating-side and advancing-side tracer particles  
 509 is displayed in Fig. 5(a-b), respectively. The tracer particles  
 510 displayed in these figures are initially located in a plane which  
 511 is halfway between the top and bottom surfaces of the work-  
 512 piece. For improved clarity, tracer-particle trajectories are color  
 513 coded. The results displayed in Fig. 5(a-b) clearly revealed the  
 514 following basic aspects of the FSW process: (a) the work-  
 515 piece material at the retreating side (as represented by the  
 516 yellow and green tracer-particle trajectories, Fig. 5a), does not,  
 517 for the most part, enter the stir zone under the tool-shoulder  
 518 and usually only flows around it; (b) the material at the  
 519 advancing side (as represented by the white and cyan tracer-  
 520 particle trajectories, Fig. 5b), which is initially close to the  
 521 butting surfaces, passes over to the retreating side and is  
 522 co-stirred with some of the retreating-side material to form  
 523 the welded joint; and (c) the advancing-side material further  
 524 away from the initial butting surfaces remains on the advancing  
 525 side and either enters the stir region on the advancing side or  
 526 flows around it.

527 *Material Hardness Field.* Variation of the material hardness  
 528 measured transversely across the friction stir weld over the top  
 529 surface of the work-piece consisting of solution-strengthened  
 530 and strain-hardened AA5083-H131 plates on both sides of the  
 531 joint is displayed in Fig. 6(a-b). The results displayed in these  
 532 two figures correspond to two different welding tool traverse  
 533 speeds: (a) Figure 6(a) 100 mm/min; and (b) Fig. 6(b),  
 534 150 mm/min, while the tool rotation speed, shoulder diameter,  
 535 and threaded pin diameter are kept constant at 350 rpm, 18  
 536 and 5 mm, respectively.

537 For comparison, the corresponding experimental results  
 538 obtained in Ref 28 are also displayed in Fig. 6(a-b). Since the  
 539 original hardness results reported in Ref 28 were given using  
 540 Vickers hardness units, they were converted using the known  
 541 indentation loads and indenter geometry data to the SI stress  
 542 units before including in these figures.

543 Simple examination of the results displayed in Fig. 6(a-b)  
 544 shows that:

- (a) The computational model developed in Ref 26 yields a  
 545 physically realistic variation in material hardness across  
 546 the FSW joints, i.e., the computed hardness profiles  
 547 clearly delineate the four different weld zones;  
 548
- (b) As far as the quantitative agreement between the com-  
 549 puted results and their counterparts from Peel et al.  
 550 (Ref 28) is concerned, it can be characterized as being  
 551 good to fair. Possible reasons for the observed discrepan-  
 552 cies include: (i) deficiencies in the functional relations  
 553 used to describe the contribution of various mechanisms  
 554 to material hardness; (ii) diversity and scarcity of the  
 555 relevant experimental data used for model parameteriza-  
 556 tion; and (iii) potential inaccuracies associated with  
 557 hardness measurements in Ref 28.  
 558

559 A comparison of the computed results (pertaining to the  
 560 hardness variation in a direction transverse to the original weld

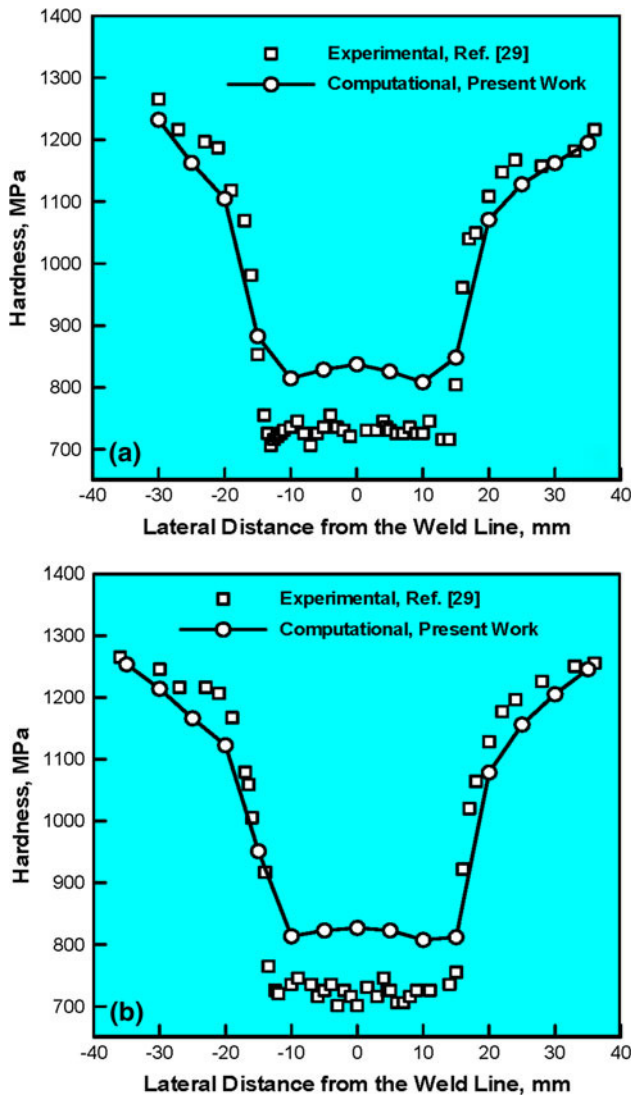


**Fig. 6** A comparison between the computed and the experimental hardness (transverse) profiles over the top surface of the 5083 work piece. Please see the text for details regarding the friction stir weld parameters associated with the results displayed in (a) and (b). Data pertaining to the advancing side of the weld joint are on the right-hand side of the plot

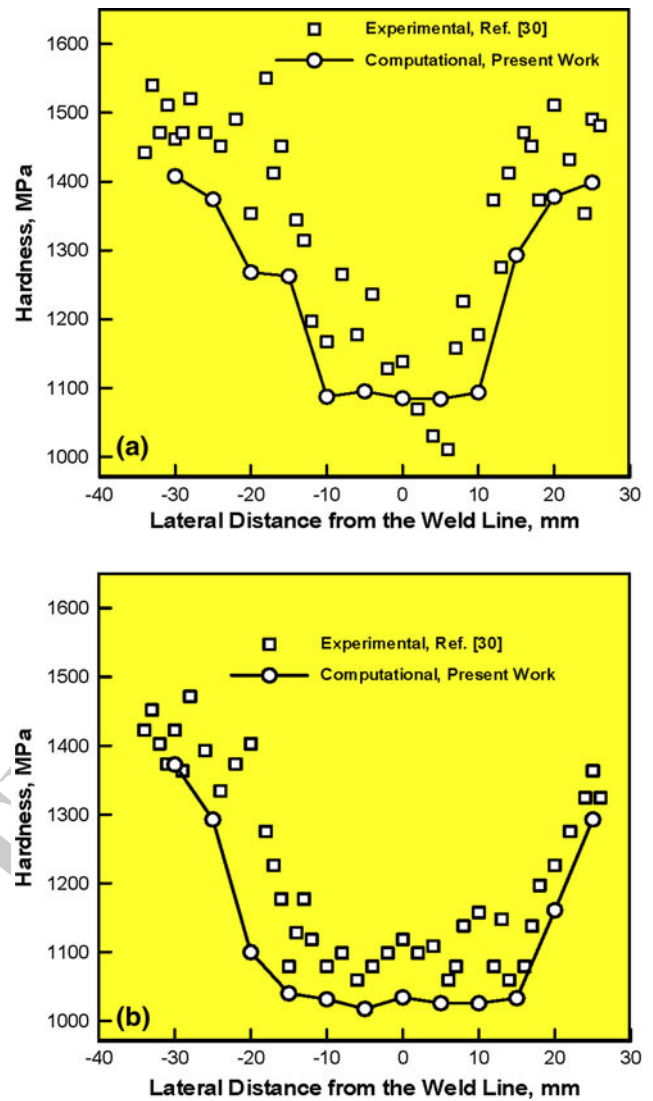


**Fig. 7** A comparison between the computed and experimental hardness profiles over a transverse cut through the 2139 work piece weld: (a) top surface of the work piece and (b) the bottom surface of the work piece. Please see the text for details regarding the friction stir welding parameters. Data pertaining to the advancing side of the weld joint are on the right-hand side of the plot

561 line) and their experimental counterparts obtained in Ref 29 in  
 562 the case of two friction-stir-welded age-hardened AA2139  
 563 plates is displayed in Fig. 7(a-b). The results displayed in  
 564 Fig. 7(a-b) correspond, respectively, to the hardness measure-  
 565 ments over the top and bottom surfaces of the work piece. In  
 566 both cases the same FSW process parameters (welding speed:  
 567 100 mm/min; tool rotational speed: 350 rpm; shoulder diam-  
 568 eter: 18 mm; and pin diameter: 5 mm) were used.

569 Simple examination of the results displayed in Fig. 7(a-b)  
 570 shows that as in the case of AA5083, the computational model  
 571 developed in Ref 26 provides physically realistic hardness  
 572 profiles in a direction transversely oriented with respect to the  
 573 weld (at different locations through the thickness of the  
 574 work-piece).

575 *Material Grain-Size Field.* A comparison between the grain-  
 576 size results obtained computationally in Ref 26 and their

577 experimental counterparts reported in Ref 30 is displayed  
 578 in Fig. 8. Considering the fact that not all the FSW process  
 579 parameters were specified in Ref 30, the level of agreement  
 580 observed in Fig. 8 can be judged as reasonable.

581 A comparison of the computed variation in the average  
 582 grain-size across the FSW joint (Ref 26) and its experimental  
 583 counterpart obtained in Ref 31 is displayed in Fig. 9. These  
 584 results pertain to the top surface of the work-piece. Simple  
 585 examination of the results displayed in Fig. 9 shows that the  
 586 computation/experiment agreement is comparable to that  
 587 obtained in the case of AA5083 (i.e., the agreement is  
 588 reasonable).

589 *Residual Stress Field.* A comparison between the computed  
 590 (Ref 26) and the experimentally measured (Ref 28) results  
 591 pertaining to variation of the longitudinal and transverse  
 592 residual stresses as a function of the distance from the initial  
 593

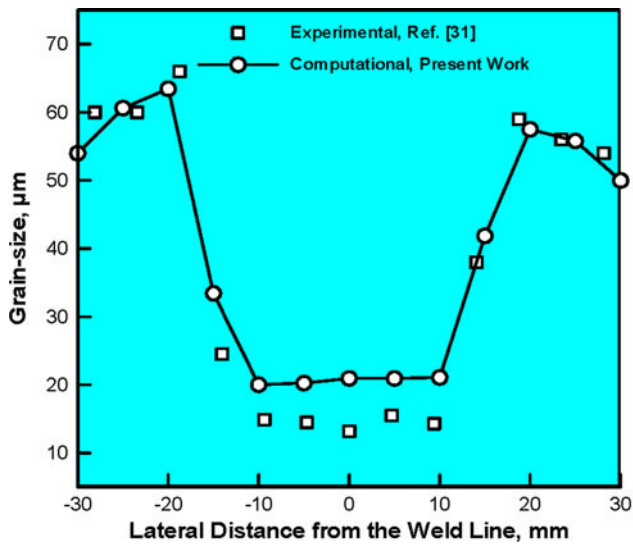


**Fig. 8** A comparison between the computed and experimental grain-size profiles over the top surface of the 5083 work piece. Data pertaining to the advancing side of the weld joint are on the right-hand side of the plot

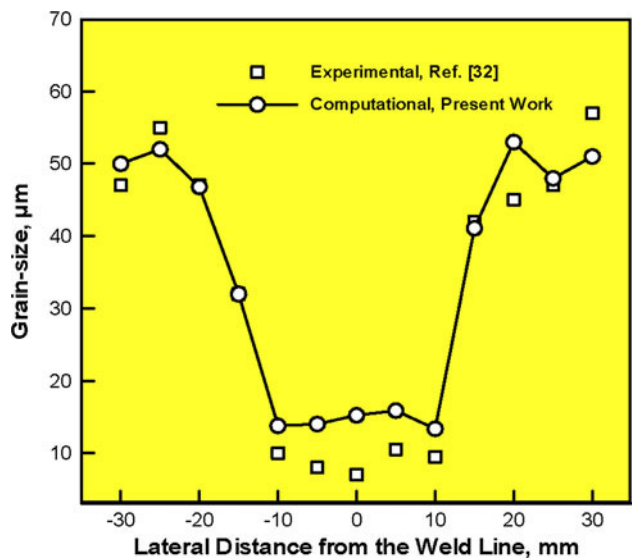


**Fig. 9** A comparison between the computed and experimental grain-size profiles over the top surface of the 2139 work piece. Data pertaining to the advancing side of the weld joint are on the right-hand side of the plot

593 location of the butting surfaces in AA5083 is displayed  
 594 in Fig. 10(a-b). Two sets of computational results are presented:  
 595 one based on the use of the original Johnson-Cook material model  
 596 while the other was based on the use of the modified  
 597 Johnson-Cook model (Ref 26). Simple examination of the  
 598 results presented in Fig. 10(a-b) shows that the results based  
 599 on the modified Johnson-Cook model are in better agreement  
 600 with the experimental results. While some disagreement still exists  
 601 between the computational results based on the modified  
 602 Johnson-Cook model and the experimental results, the overall  
 603 residual stress distribution profile appears to be reasonably

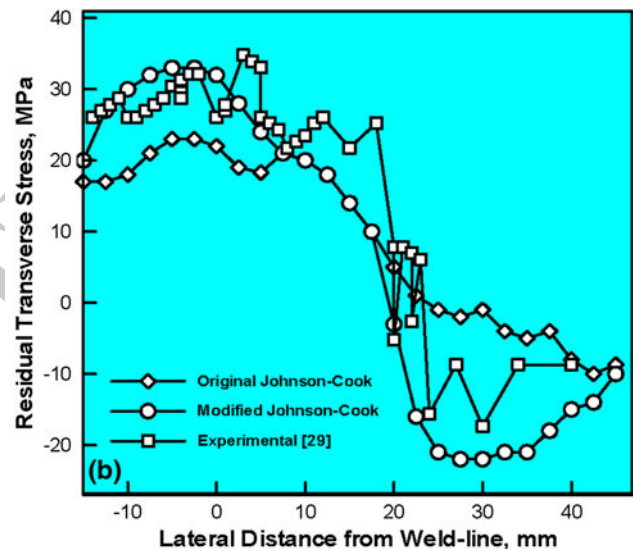
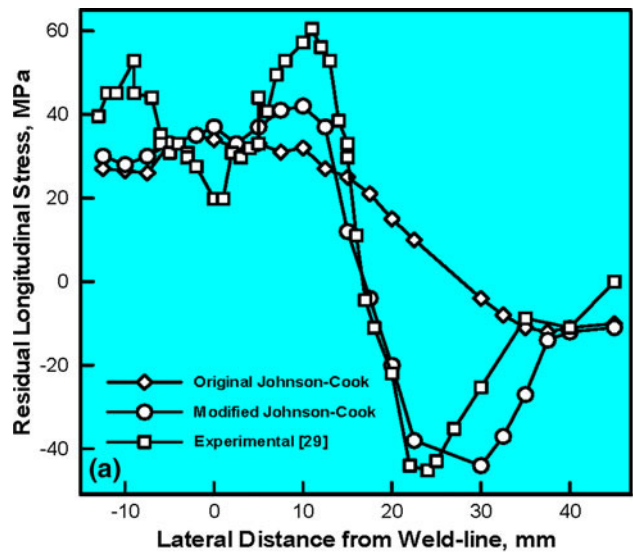


**Fig. 10** Variation of the: (a) longitudinal and (b) transverse residual stresses as a function of the distance from the weld-line in 5083. Data pertaining to the advancing side of the weld joint are on the right-hand side of the plot

well reproduced by the computational analysis (Ref 26). Specifically:

- (a) The residual stresses are compressive at larger distances from the weld-line at the advancing side of the weld (the right-hand side in Fig. 10a-b);
- (b) As one approaches the weld-line at the advancing side, the residual stresses first increase in magnitude and then switch their character (i.e., becomes tensile), at a distance of 15-20 mm from the weld-line (at the advancing side);
- (c) In the innermost portion of the nugget, the tensile residual stresses tend to decrease somewhat;
- (d) As the distance from the weld-line increases on the retreating side, the stresses gradually decrease toward zero; and
- (e) The longitudinal residual stresses are generally higher than their transverse counterparts.

When coupled with conventional Design of Experiments (DOE) and/or Design Optimization (DO) techniques, the experimental and computational analyses overviewed in the previous section can be used to identify an optimal combination of the FSW process parameters and tool design geometrical/material parameters for a given choice of the aluminum-alloy grades and plate thicknesses. While attempting to identify optimal FSW process and weld-tool parameters, the emphasis is placed on maximizing the manufacturing efficiency of the joining process (as quantified by the tool travel speed), maximizing the quality of the FSW joint (as quantified by the material mechanical properties and their consistency) and minimizing the forces which must be applied to the tool and the work piece during the welding process (primarily the axial tool-driving and the transverse work-piece clamping forces).

**2.4.1 FSW Process Optimization.** The optimal FSW process parameters (for a given tool design and the choice of the aluminum-alloy grades and plate thicknesses), are generally determined by employing the computational analyses like the one reported in Ref 26. An example output from such analyses is displayed in Fig. 11 in which a thermal foot-print at the front and rear of the shoulder of the weld tool are shown. Temperature distribution within the foot-print and the knowledge of the material solidus temperature (the lowest temperature at which melting is observed) and the effect of temperature on the material strength are used to determine the optimal FSW process parameters.

This procedure typically reveals that (for a given tool design, the rotational speed of the tool and the choice of the aluminum alloy grades and plate thicknesses), there is an optimal range of the tool traverse speeds. Tool travel speeds exceeding this range typically give rise to the formation of low-ductility flaws within the weld, while, for tool speeds below this

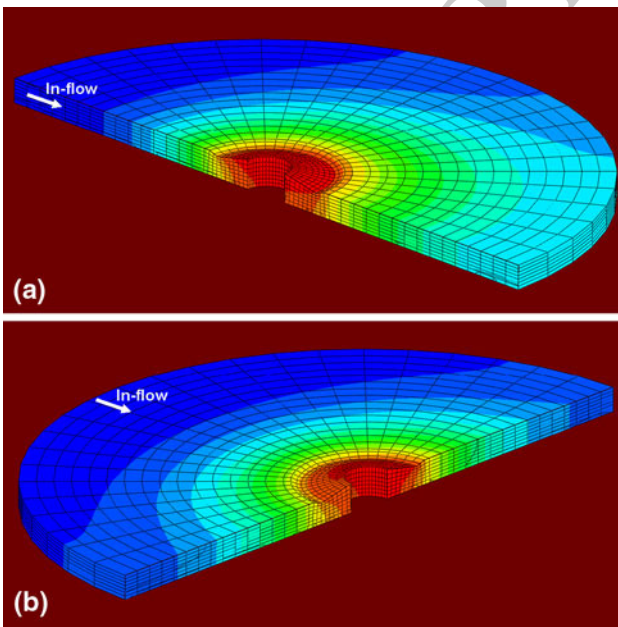


**Fig. 11** Typical temperature distribution over one-half of the work-piece obtained by cutting along: (a) the longitudinal; and (b) transverse directions: Maximum (red) = 400 °C; Minimum (blue) = 25 °C

range, microstructural defects associated with excessive heating are often observed. Within this range lower velocities typically cause HAZ to possess over-aging induced inferior microstructure/properties (i.e., welds typically fracture in this weld zone). On the other hand, in the upper region of the optimal tool-speed range, failure typically occurs within the weld nugget region (since, material over-aging within the HAZ is less pronounced and the properties less degraded).

**2.4.2 FSW Tool-Design Optimization.** The problem of finding the optimal design of the weld tool is generally quite challenging since the tool geometry can be quite complex and entails a large number of parameters for its full description. Typically, there is an optimal pin length an optimal pin-diameter to pin-length ratio as well as an optimal pin-diameter to shoulder-diameter ratio. In addition to these tool design parameters, there is a relatively large number of parameters which describe the pin shape (i.e., thread, flute, frustum with flats, etc.), and the shoulder shape (scroll, spiral etc.).

Typically, when high strength aluminum alloys are FSWed, the optimal weld-tool design involves a flat ended threaded, frustum-shaped pin profile with three-four equally spaced flats machined into the profiled surfaces and a scroll or spiral shoulder profile, Fig. 12. The flat end of the pin helps to produce a better stir zone or weld nugget penetration to the back of the work-piece. The threaded portion of the pin body promotes material transport in the work-piece through-the-thickness direction while the frustum-shaped pin profile promotes material extrusion around the tool and its forging in the region behind the tool. The scroll shoulder design enables welding without tilting the welding tool relative to the work-piece, which facilitates welding around corners.

### 3. FSW Weld Joint Design and Testing

#### 3.1 Design Considerations for the FSW Joints

**3.1.1 90° Corner Joints.** Construction of complex structural components such as military-vehicle underbodies/hulls typically involves not only in-plane (planar) but also out-of-plane (e.g., corner) joint configurations. Hence, one of the challenges associated with the construction of these structures

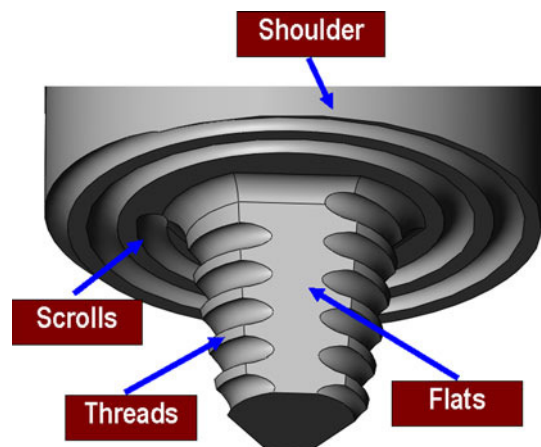


**Fig. 12** Typical optimal design of the FSW tool used for joining high-strength aluminum-alloy grades

693 is determination of the optimal weld joint configuration(s). For  
 694 example, in the case of corner FSW joints, like the one  
 695 associated with the joining of the vehicle floor section to the  
 696 frame sidewalls, one can choose between a butted corner joint,  
 697 Fig. 13(a), and a rabbeted corner joint, Fig. 13(b). Furthermore,  
 698 in the latter case, the joint is characterized by a single  
 699 geometrical design parameter (the rabbet depth), Fig. 13(b).

700 Each of the two aforementioned corner joints possess certain  
 701 advantages and shortcomings, e.g., while the butted corner joint  
 702 requires less pre-weld preparation (i.e., less or no machining is  
 703 required for preparation of the weld surfaces), it entails special  
 704 tooling in-order to support the horizontal weld plate, Fig. 13(a).  
 705 On the other hand, in the case of the rabbet corner weld joint  
 706 which is commonly used in conventional arc welding, fixturing  
 707 is less challenging but a segment between the horizontal and  
 708 vertical members is left un-welded, Fig. 13(b). To obtain load  
 709 transfer between the horizontal and vertical members in this  
 710 region, it is a common arc welding practice to deposit a fillet  
 711 weld along the inner edge. As shown in Fig. 14, FSW also  
 712 enables formation of a seam weld along the inner edge.

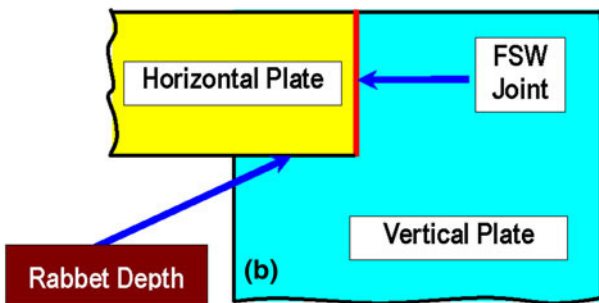
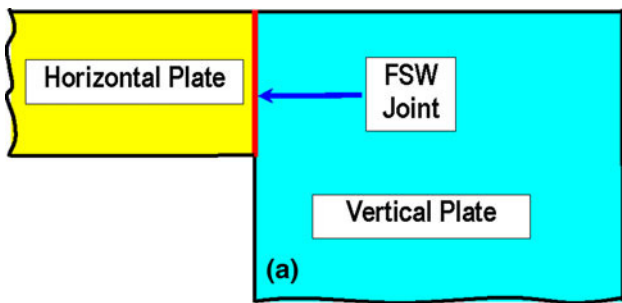


Fig. 13 Two designs of corner joints most often in conjunction with the FSW process: (a) butted corner joint; and (b) rabbeted corner joint

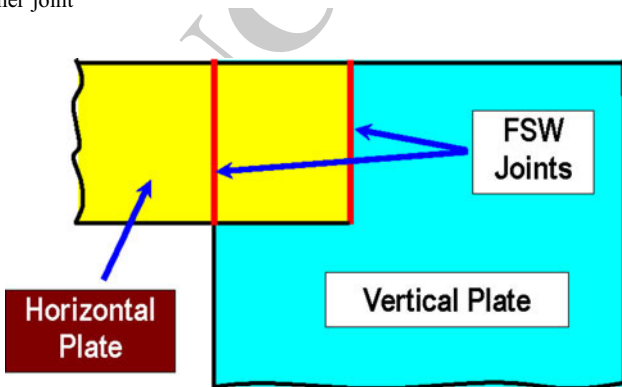


Fig. 14 Joining of the 90° angled plates along their inner edge using FSW

713 To identify the optimal FSW corner-joint configuration, it  
 714 is a common practice to fabricate and test these joints.  
 715 While, the mechanical response of these joints when  
 716 subjected to a variety of loading conditions can be, in  
 717 principle, assessed computationally, these types of computa-  
 718 tional analyses are not frequently employed. Instead, the  
 719 welds are qualified almost exclusively using experimental  
 720 means (e.g., the so called ballistic shock test described in the  
 721 next section).

722 **3.1.2 Low Angle Out-of-Plane Joints.** Military-vehicle  
 723 underbody/hull constructions often involve low angle out-of-  
 724 plane joints (e.g., V-shaped hulls). While, it is, in principle,  
 725 possible to produce such joints by directly welding the  
 726 angled plates, the welding process is quite challenging and  
 727 the weld quality is often deficient. Consequently, it is  
 728 suggested that machined or extruded angular transition  
 729 members be used in this case and that a single low-angle  
 730 out-of-plane joint be replaced by two planar butt joints,  
 731 Fig. 15(a) and (b).

732 **3.1.3 Complex Three-Dimensional Weld Joints.** Due to  
 733 high complexity of the military-vehicle underbody/hull  
 734 constructions, FSW weld tool is often required to follow  
 735 intricate three-dimensional trajectories. Under such circum-  
 736 stances, it is advantageous that the tool remains normal to  
 737 the outer surface of the plates being welded. As mentioned  
 738 earlier, this can be attained, while ensuring a high quality of  
 739 the weld, by using a scrolled shoulder. Also, to prevent the  
 740 relative motion of the plates being welded and to ensure  
 741 good dimensional accuracy it is suggested that the sections  
 742 being joined be Friction-stir tack welded prior to being  
 743 FSWed.

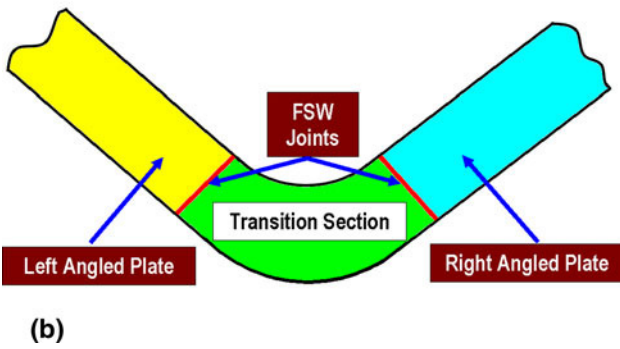
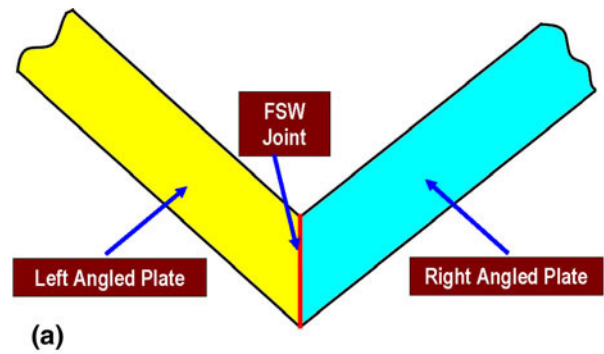
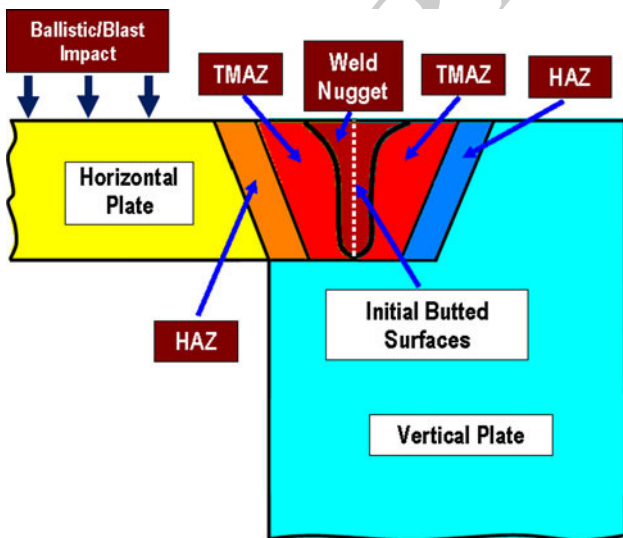


Fig. 15 Two possible designs for a low angle out-of-plane joints. A single low angle out-of-plane joint in (a) is replaced (with the help of an angular transition section) into two planar butt joints in (b)

When the ability of FSW joints to withstand high-rate loading is of primary concern, these welds are typically subjected to the so called ballistic shock impact test as defined in MIL-STD-1946A (Ref 32). In accordance with this test, the weld joint is impacted by a 75 mm-diameter/150 mm-length solid right circular cylindrical aluminum slug at a velocity defined by the attendant aluminum alloy grades and plate thicknesses. For the weld to qualify, the total crack length must not exceed 305 mm.

When the ballistic shock test is used to qualify butted corner and rabbeted corner FSW joints, clear differences between these two types of weld designs are often observed. That is, the butted corner joint is often found to out perform the rabbeted corner joint with respect to the ballistic shock loading. This finding may have significant economical benefits since the use of the butted corner joint reduces the production costs by eliminating the need for pre-weld machining of the rabbet.

The aforementioned differences between the two corner-joint designs can be rationalized as follows: (a) In the case of the inferior rabbeted-corner joint, the HAZ was often found to extend across the inner most edge of the two plates where, under dynamic loading conditions, shear stresses are the highest, Fig. 16. Since, in this case, the over-aged inferior HAZ microstructure is located in the region associated with the most severe loading, it is no surprise that rabbeted corner joints possess sub-standard ballistic performance. It should be noted, however, that the actual location of the HAZ can be changed by modifying the rabbet depth which would result in an improved ballistic performance of the rabbeted corner joint; and (b) In the case of the butted corner joints, fine grained weld nugget zone with superior impact strength is typically placed in the region of highest shear stresses. Since, fine grain microstructure is highly beneficial to dynamic strength of the material; the superior ballistic performance of the butted joint is justified.



**Fig. 16** A possible reason for the inferior ballistic performance of rabbeted corner joints, i.e., the HAZ which contains degraded over-aged material is located in the region experiencing maximum shear stresses

Within the third stage of introduction of the FSW process in the construction of military vehicle underbodies/hulls, a sub-scale test structure is typically fabricated and tested under fairly realistic buried-mine blast loading conditions. The test structure is normally required to meet stringent conditions pertaining to the absence of penetration/fragmentation and a lack of excessive deflections. An example of the vehicle-hull test structure used in our work is displayed in Fig. 17. Due to the sensitive nature of the subject matter details regarding this test structure and its blast survivability potential could not be discussed here.

#### 4.1 Design Consideration for the FSW Joints

When designing the test structures, it is critical to ensure that their topology and design (e.g., plates, stiffeners, and structural details) closely resemble those of prototypical military vehicles so that the results obtained can be used to judge blast survivability of the vehicle structures themselves. In addition, during fabrication of the test structures, the proper FSW practice discussed in Section 2 should be exercised in order to produce high quality flat, corner, and low-angle weld joints. Failure to do so may provide wrong/misleading information regarding the feasibility for utilizing high strength aluminum alloys and the FSW technique in manufacturing blast-survivable military-vehicle structures.

#### 4.2 Buried-Mine Blast Testing of FSWed Military-Vehicle Test Structures

The ultimate proof for suitability of the FSW technology and high-strength aluminum alloys for use in military-vehicle underbody/hull structures is obtained during the mine-blast survivability testing stage. Within this stage, the vehicle-hull test structure is secured within a test fixture and subjected to blast loads resulting from detonation of a mine buried in soil. Since during this process a sub-scale vehicle underbody test structure is tested, the following problems must be resolved before the test results can be used to quantify blast survivability of the military vehicles in question:

- The manner in which the test structure is secured to the test fixture and the overall fixture weight should closely resemble their counterparts present in the vehicle.

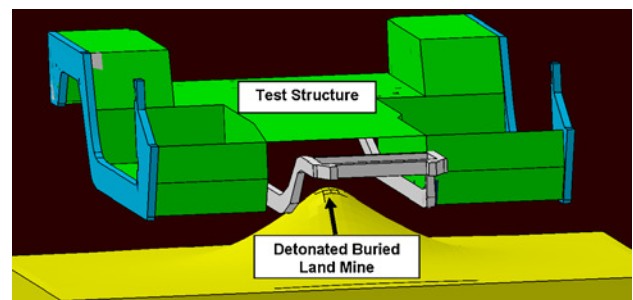


**Fig. 17** An example of the sub-scale vehicle underbody/hull test structure used in mine-blast experiments in order to assess suitability of the FSW process for the fabrication of high-survival military vehicles

- 819 This is a critical requirement since often the performance  
 820 of structures (including joints) is greatly affected by the  
 821 effect of surrounding constraints/interactions;  
 822 (b) If the test structure is sub-scaled then a dimensional  
 823 analysis should be employed to account for the scaling  
 824 effects (e.g. Ref 33);  
 825 (c) While a full-factorial blast-testing schedule over the  
 826 design/test variables (mine size, shape and explosion  
 827 energy, depth of burial, stand-off distance, soil type,  
 828 compaction level, and degree of saturation, etc.) is pre-  
 829 ferred, in many cases blast testing under most adverse  
 830 combinations of these test variables may suffice; and  
 831 (d) A comprehensive failure analysis should be conducted  
 832 following each mine-blast test. Past experience has  
 833 shown that one can learn a great deal about the behavior  
 834 of materials and structures by investigating the manner  
 835 in which they fail in the presence of various loading  
 836 and constraining conditions.

## 5. Summary Remarks

837 In the present article, a procedure is developed for the  
 838 introduction of friction stir welding (FSW) technology and  
 839 high-strength age-hardened aluminum alloys to the construction  
 840 of blast-survivable military-vehicle underbody/hull structures.  
 841 The procedure involves three basic steps, Fig. 18.

842 Within the first step, various experimental and computa-  
 843 tional methods are employed in order to optimize the FSW  
 844 process and the weld-tool design with respect to attaining high  
 845 productivity of the welding process, high quality of the weld  
 846 (i.e., low defect content and superior mechanical properties of  
 847 the weld material) and low axial (tool driving) and transverse  
 848 (work-piece clamping) forces required for the FSW process.  
 849

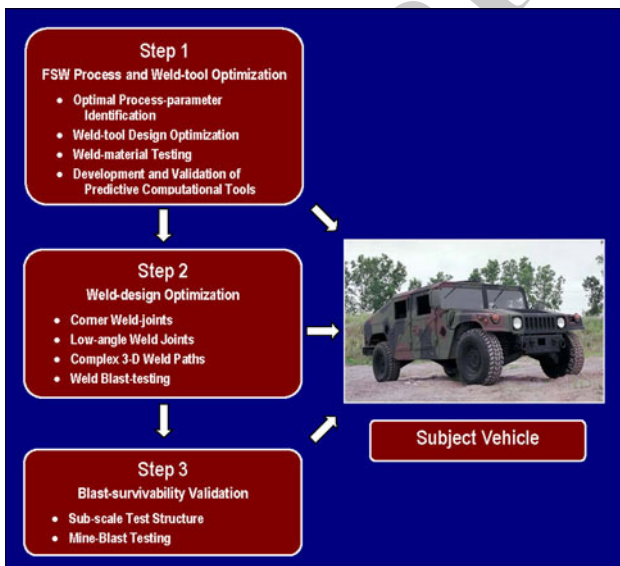


**Fig. 18** A three-step procedure for the introduction of friction stir welding (FSW) technology and high-strength age-hardened aluminum alloys to the construction of blast-survivable military-vehicle underbody hull structures

850 Within the second step, various FSW-joint designs are  
 851 considered in order to identify the optimal design for different  
 852 joints encountered during construction of the military-vehicle  
 853 underbody/hull structures. Typical procedures used to qualify  
 854 individual weld joints with respect to dynamic loads as those  
 855 accompanying mine blast are also considered.

856 In the third step, fully fabricated (sub-scale) military-  
 857 vehicle underbody/hull test structures are subjected to mine-  
 858 blast loads in order to assess their level of blast survivability.  
 859 The key aspects of test structures fabrication and testing as  
 860 well as of the data reduction (including the scaling effects) are  
 861 also discussed.

## Acknowledgments

862 The material presented in this article is based on work  
 863 supported by the U.S. Army/Clemson University Cooperative  
 864 Agreements W911NF-04-2-0024 and W911NF-06-2-0042 and by  
 865 the Army Research Office sponsored Grant W911NF-09-1-0513.  
 866

## References

- 867
- 868 1. W.M. Thomas, E.D. Nicholas, J.C. Needham, M.G. Murch, P. Temple-  
 869 Smith, and C.J. Dawes, "Friction Stir Butt Welding," International  
 870 Patent Application No. PCT/GB92/02203, 1991
  - 871 2. "Armor Plate, Aluminum Alloy, Weldable 5083 and 5456," MIL-  
 872 DTL-46027J, U.S. Department of Defense, Washington DC, August  
 873 1992
  - 874 3. A. Cho, Alcan Rolled Products, Ravenswood, WV, USA, Private  
 875 Communication, June 2009
  - 876 4. "Armor Plate, Aluminum Alloy, 7039," MIL-DTL-46063H, U.S.  
 877 Department of Defense, Washington DC, December 1992
  - 878 5. "Aluminum Alloy Armor, 2219, Rolled Plate and Die Forged Shapes,"  
 879 MIL-DTL-46118E, U.S. Department of Defense, Washington DC,  
 880 August 1998
  - 881 6. "Aluminum Alloy Armor Rolled Plate (1/2 to 4 Inches Thick),  
 882 Weldable (Alloy 2519)," MIL-DTL-46118E, U.S. Department of  
 883 Defense, Washington DC, February 2000
  - 884 7. H. Liu, H. Fulii, M. Maeda, and K. Nogi, Tensile Properties and  
 885 Fracture Locations of Friction-Stir Welded Joints of 6061-T6 Alumin-  
 886 ium Alloy, *J. Mater. Sci. Lett.*, 2003, **22**, p 1061–1063
  - 887 8. W.B. Lee, C.Y. Lee, W.S. Chang, Y.M. Yeon, and S.B. Jung,  
 888 Microstructural Investigation of Friction Stir Welded Pure Titanium,  
 889 *Mater. Lett.*, 2005, **59**, p 3315–3318
  - 890 9. W.M. Thomas and E.D. Nicholas, Friction Stir Welding for the  
 891 Transportation Industries, *Mater. Des.*, 1997, **18**, p 269–273
  - 892 10. J.Q. Su, T.W. Nelson, R. Mishra, and M. Mahoney, Microstructural  
 893 Investigation of Friction Stir Welded 7050-T651 Aluminum, *Acta*  
 894 *Mater.*, 2003, **51**, p 713–729
  - 895 11. O. Frigaard, Ø. Grong, and O.T. Midling, A Process Model for Friction  
 896 Stir Welding of Age Hardening Aluminum Alloys, *Metall. Mater.*  
 897 *Trans. A*, 2001, **32**, p 1189–1200
  - 898 12. M.W. Mahoney, C.G. Rhodes, J.G. Flintoff, R.A. Spurling, and W.H.  
 899 Bingel, Properties of Friction-Stir-Welded 7075 T651 Aluminum,  
 900 *Metall. Mater. Trans. A*, 1998, **29**, p 1955–1964
  - 901 13. C.G. Rhodes, M.W. Mahoney, W.H. Bingel, R.A. Spurling, and C.C.  
 902 Bampton, Effect of Friction Stir Welding on Microstructure of 7075  
 903 Aluminum, *Scripta Mater.*, 1997, **36**, p 69–75
  - 904 14. G. Liu, L.E. Murr, C.S. Niou, J.C. McClure, and F.R. Vega,  
 905 Microstructural Aspects of the Friction-Stir-Welding of 6061-T6  
 906 Aluminum, *Scripta Mater.*, 1997, **37**, p 355–361
  - 907 15. K.V. Jata and S.L. Semiatin, Continuous Dynamic Recrystallization  
 908 During Friction Stir Welding, *Scripta Mater.*, 2000, **43**, p 743–748
  - 909 16. K. Masaki, Y.S. Sato, M. Maeda, and H. Kokawa, Experimental  
 910 Simulation of Recrystallized Microstructure in Friction Stir Welded Al  
 911 Alloy Using a Plane-Strain Compression Test, *Scripta Mater.*, 2008,  
 912 **58**, p 355–360

- 913  
914  
915  
916  
917  
918  
919  
920  
921  
922  
923  
924  
925  
926  
927  
928  
929  
930  
931  
932  
933  
934  
935  
936  
937  
938  
939
17. J.H. Cho, D.E. Boyce, and P.R. Dawson, Modeling Strain Hardening and Texture Evolution in Friction Stir Welding of Stainless Steel, *Mater. Sci. Eng. A*, 2005, **398**, p 146–163
  18. M. Grujicic, G. Arakere, C.-F.Yen, and B.A. Cheeseman, Computational Investigation of Hardness Evolution During Friction-stir Welding of AA5083 and AA2139 Aluminum Alloys, *J. Mater. Design Appl.*, submitted for publication, November 2009
  19. W.M. Thomas, E.D. Nicholas, J.C. Needham, M.G. Murch, P. Templesmith, and C.J. Dawes, "Friction Stir Welding," International Patent Application No. PCT/GB92102203 and Great Britain Patent Application No. 9125978.8, 1991
  20. R.S. Mishra and Z.Y. Ma, Friction Stir Welding and Processing, *Mater. Sci. Eng. R Rep.*, 2005, **50**, p 1–78
  21. H.W. Zhang, Z. Zhang, and J.T. Chen, The Finite Element Simulation of the Friction Stir Welding Process, *Mater. Sci. Eng. A*, 2005, **403**, p 340–348
  22. A.J. Ramirez and M.C. Juhas, Microstructural Evolution in Ti-6Al-4V Friction Stir Welds, *Mater. Sci. Forum*, 2003, **426–432**, p 2999–3004
  23. H.G. Salem, A.P. Reynolds, and J.S. Lyons, Microstructure and Retention of Superplasticity of Friction Stir Welded Superplastic 2095 Sheet, *Scripta Mater.*, 2002, **46**, p 337–342
  24. H.J. Liu, Y.C. Chen, and J.C. Feng, Effect of Zigzag Line on the Mechanical Properties of Friction Stir Welded Joints of an Al-Cu Alloy, *Scripta Mater.*, 2006, **55**, p 231–234
  25. Z.Y. Ma, S.R. Sharma, and R.S. Mishra, Effect of Friction Stir Processing on the microstructure of Cast A356 Aluminum, *Mater. Sci. Eng. A*, 2006, **433**, p 269–278
  26. M. Grujicic, T. He, G. Arakere, H.V. Yalavarthy, C.-F.Yen, and B.A. Cheeseman, Fully-Coupled Thermo-Mechanical Finite-Element Investigation of Material Evolution During Friction-Stir Welding of AA5083, *J. Mater. Eng. Perform.*, accepted for publication, June 2009
  27. G. Campbell and T. Stotler, Friction-stir Welding of Armor Grade Aluminum Plate, *Welding J.*, 1999, **78**(12), p 4547
  28. M. Peel, A. Steuwer, M. Preuss, and P.J. Withers, Microstructure, Mechanical properties and Residual Stresses as a function of Welding Speed in Aluminium AA5083 Friction Stir Welds, *Acta Mater.*, 2003, **51**, p 4791–4801
  29. D. Allehaux and F. Marie, Mechanical and Corrosion Behavior of the 2139 Aluminum-Copper-Alloy Welded by the Friction Stir Welding Using the Bobbin Tool Technique, *Mater. Sci. Forum*, 2006, **519–521**, p 1131–1138
  30. Y.S. Sato, S. Hwan, C. Park, and H. Kokawa, Microstructural Factors Governing Hardness in Friction-Stir Welds of Solid-Solution-Hardened Al Alloys, *Metall. Mater. Trans. A*, 2001, **32A**, p 3033–3042
  31. L. Fratini, G. Buffa, and D. Palmeri, Using a Neural Network for Predicting the Average Grain-Size in Friction Stir Welding Processes, *Comput. Struct.*, 2009, **87**, p 1166–1174
  32. "Military Standard for Welding of Aluminum Alloy Armor," MIL-STD-1946A, U.S. Department of Defense, Washington DC, January 1990
  33. A. Wenzel and J.M. Hennessey, Analysis and Measurements of the Response of Armor Plates to Land Mine Attacks, *Proceedings of the Army Symposium on Solid Mechanics*, Warren, Michigan, July 1972, p 114–128
- 940  
941  
942  
943  
944  
945  
946  
947  
948  
949  
950  
951  
952  
953  
954  
955  
956  
957  
958  
959  
960  
961  
962  
963  
964  
965  
966  
967